Supplementary Materials for:

Chloroplast precursor protein preClpD overaccumulation triggers multilevel reprogramming of gene expression and heat shock-like responses

Zheng-Hui Hong[1], Liyu Zhu[1], Lin-Lin Gao[1], Zhe Zhu[2], Tong Su[1], Leonard Krall[2], Xu-Na Wu[2], Ralph Bock[3], and Guo-Zhang Wu[1]*

[1]Shanghai Collaborative Innovation Center of Agri-Seeds, Joint Center for Single Cell Biology, School of Agriculture and Biology, Shanghai Jiao Tong University, 800 Dongchuan Rd., 200240, Shanghai, China

[2]School of Life Sciences, Yunnan University, Kunming, Yunnan Province, China

[3]Max-Planck-Institut für Molekulare Pflanzenphysiologie, Am Mühlenberg 1, D-14476 Potsdam-Golm, Germany

*Corresponding author: Guo-Zhang Wu (gzwu@sjtu.edu.cn)

Contents:

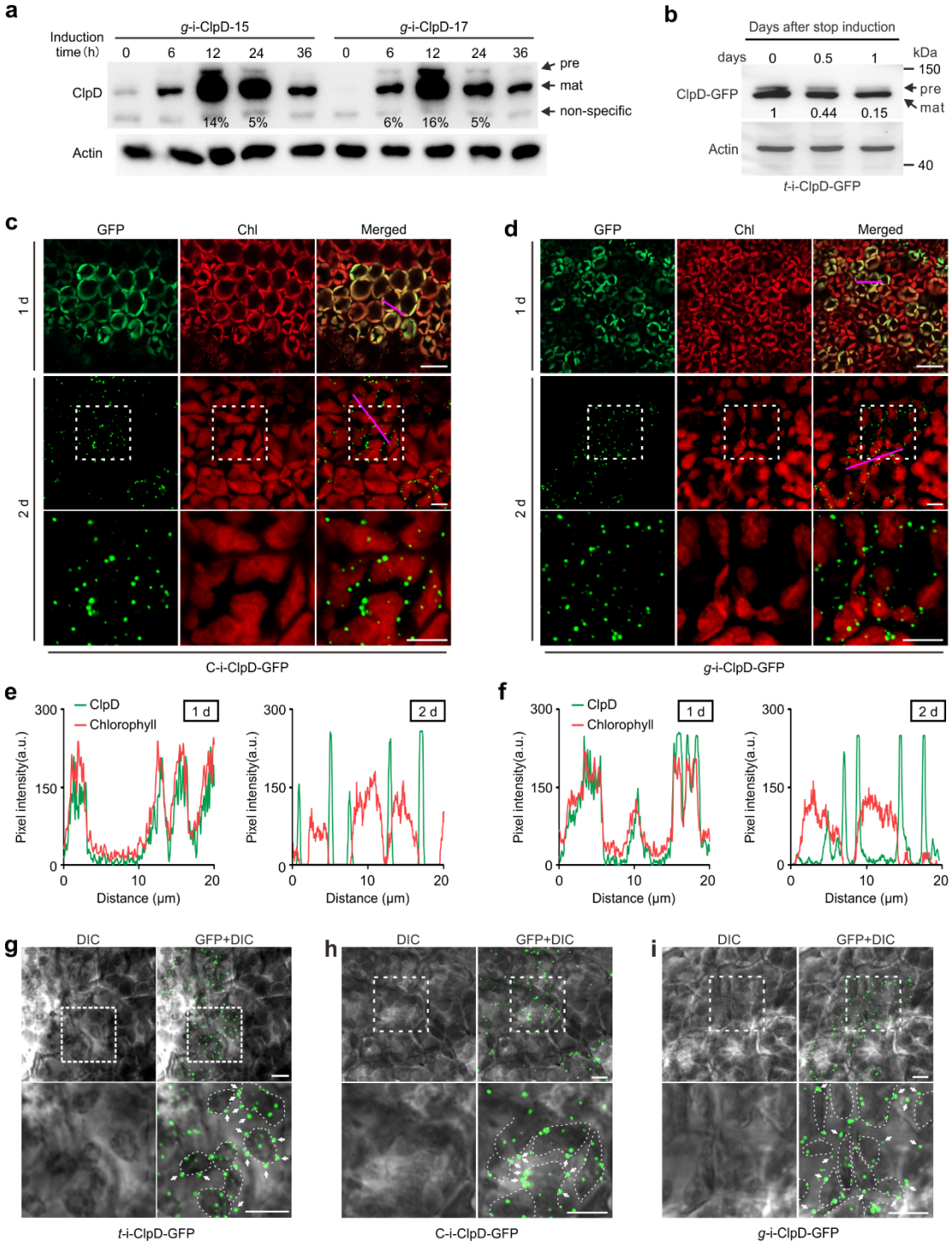

Supplementary Fig. 1 | Precursor granules are closely distributed with chloroplasts in the C-i-ClpD-GFP and *g*-i-ClpD-GFP lines.

a Time course of induction of inducible ClpD expression (without a GFP tag) in the *gun1* background (*g*-i-ClpD). The (pre)ClpD protein starts to accumulate at 6 h, peaks at 12 h of induction, and then quickly declines. Six-d-old seedlings were used for induction and the whole seedlings were harvested for analyses. The numbers below the ClpD immunoblot represent the accumulation of preClpD relative to mature ClpD (in %). Actin served as loading control. pre, preClpD; mat, mature ClpD. **b** The

precursor of ClpD-GFP declined after removal of induction reagent. Six-d-old of the *t*-i-ClpD-GFP seedlings were induced for another 4 days and then were moved to a growth chamber without ethanol for the time indicated. Whole seedlings were harvested for analyses. The relative preClpD-GFP abundances were shown below the immunoblot, which were compared to the time point when the induction was just stopped (0 d) and normalized to the loading control of Actin. **c,d** Representative images showing that the preClpD-GFP granules are closely distributed with chloroplasts in the C-i-ClpD-GFP and *g*-i-ClpD-GFP lines. Seven-day-old seedlings were induced for 1 or 2 days and the newly emerged true leaves were analyzed by confocal microscopy. Boxed areas were magnified and are shown below. Scale bars, 20 μm for the upper panel, and 5 μm for the middle and bottom panels (2 days). **e,f** Fluorescence intensity plots along the magenta lines in **c** and **d** for C-i-ClpD-GFP (**e**) and *g*-i-ClpD-GFP (**f**), respectively. The GFP and chlorophyll fluorescence intensities were measured by using Fiji software. **g-i** The differential interference contrast (DIC) images were merged with GFP of 2 days induced *t*-i-ClpD-GFP in Fig. 2b (**g**), C-i-ClpD-GFP in panel **c** (**h**), *g*-i-ClpD-GFP in panel **d** (**i**). The boundaries of chloroplasts were marked with dotted lines according to the DIC images. The preClpD-GFP granules (outside of chloroplasts) are indicated with arrows. Scale bars, 5 μm.

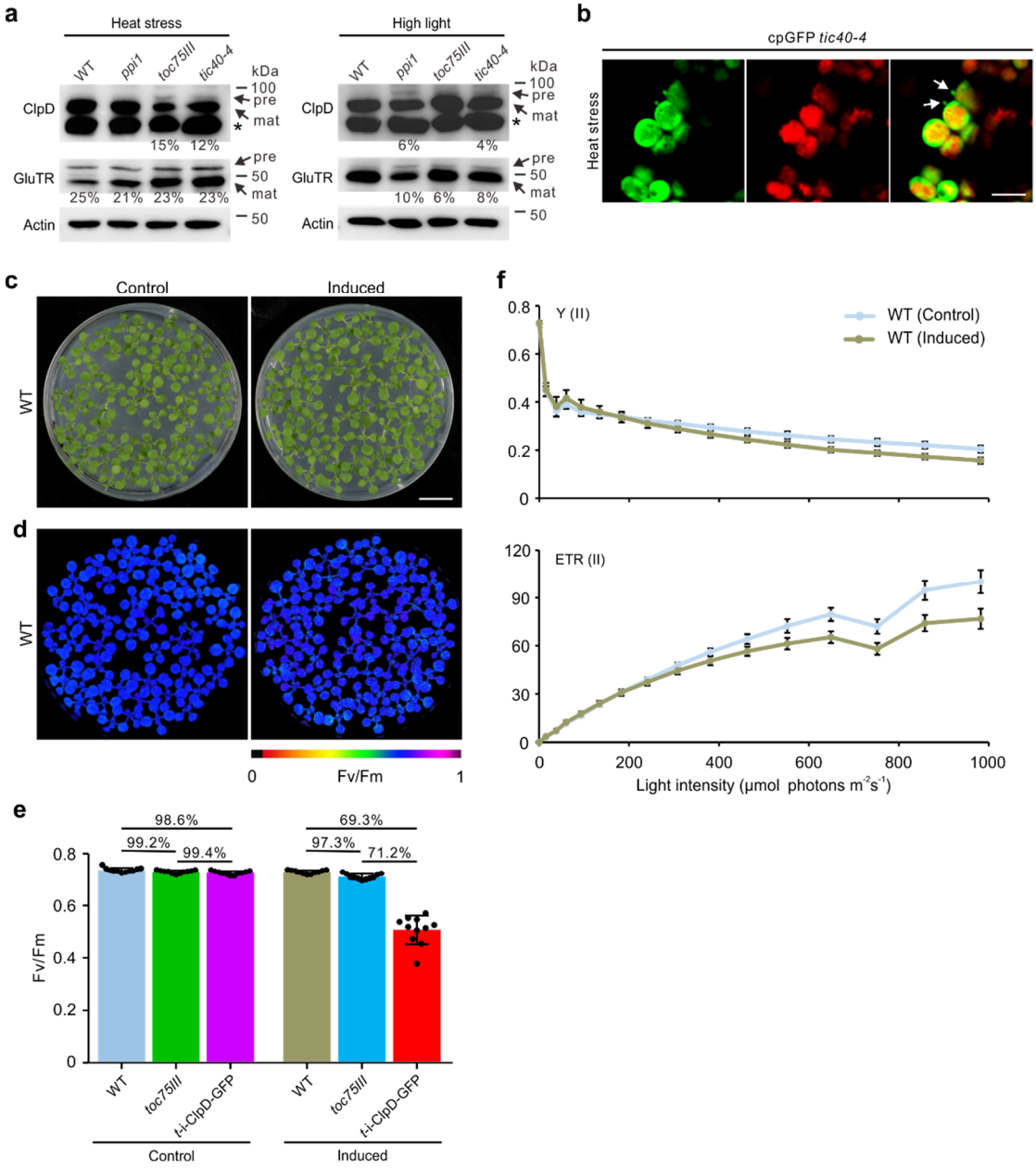

Supplementary Fig. 2 | Accumulation of chloroplast precursors under abiotic stress conditions and the photosynthetic capacity of the WT w/wo induction.

a Precursors of ClpD and GluTR accumulated in the chloroplast protein import-related mutants, *ppi1*, *toc75III*, and *tic40-4*, under heat or high light stress. Note, that preGluTR also accumulated in the WT seedlings under heat stress. The numbers below the ClpD and GluTR immunoblots represent the accumulation of precursors relative to the mature proteins (in %). Six-d-old seedlings from different genotypes were treated with heat stress (37 °C) for 5 days or high light stress (500 μmol photos m^{-2} s^{-1}) for 6 days. Asterisks indicate nonspecific crossreations of the ClpD antibody. Actin served as load controls. **b** pre-cpGFP granules accumulated in the *tic40-4* mutant after heat stress. The granules were in close approximity to the chloroplasts. Six-d-old of cpGFP *tic40-4*

seedlings were treated with heat stress (37 ℃) for additional 1 day. Scale bar, 5 μm. In **a** and **b**, true leaves were used for analyses. **c-f** The growth phenotype (**c**), Fv/Fm images of the WT (**d**), quantified Fv/Fm from different genotyoes (**e**), and light-response curves of chlorophyll *a* fluorescence parameters of the WT (**f**) after 2 days of induction. Six-d-old seedlings were used for induction. In **c**, scale bar, 1 cm. In **e**, data are means ± SD from 11 biological replicates. The relative values (in %) of Fv/Fm of the *toc75III* and *t*-i-ClpD-GFP to that of the WT, or the *t*-i-ClpD-GFP to that of the *toc75III* were indicated.

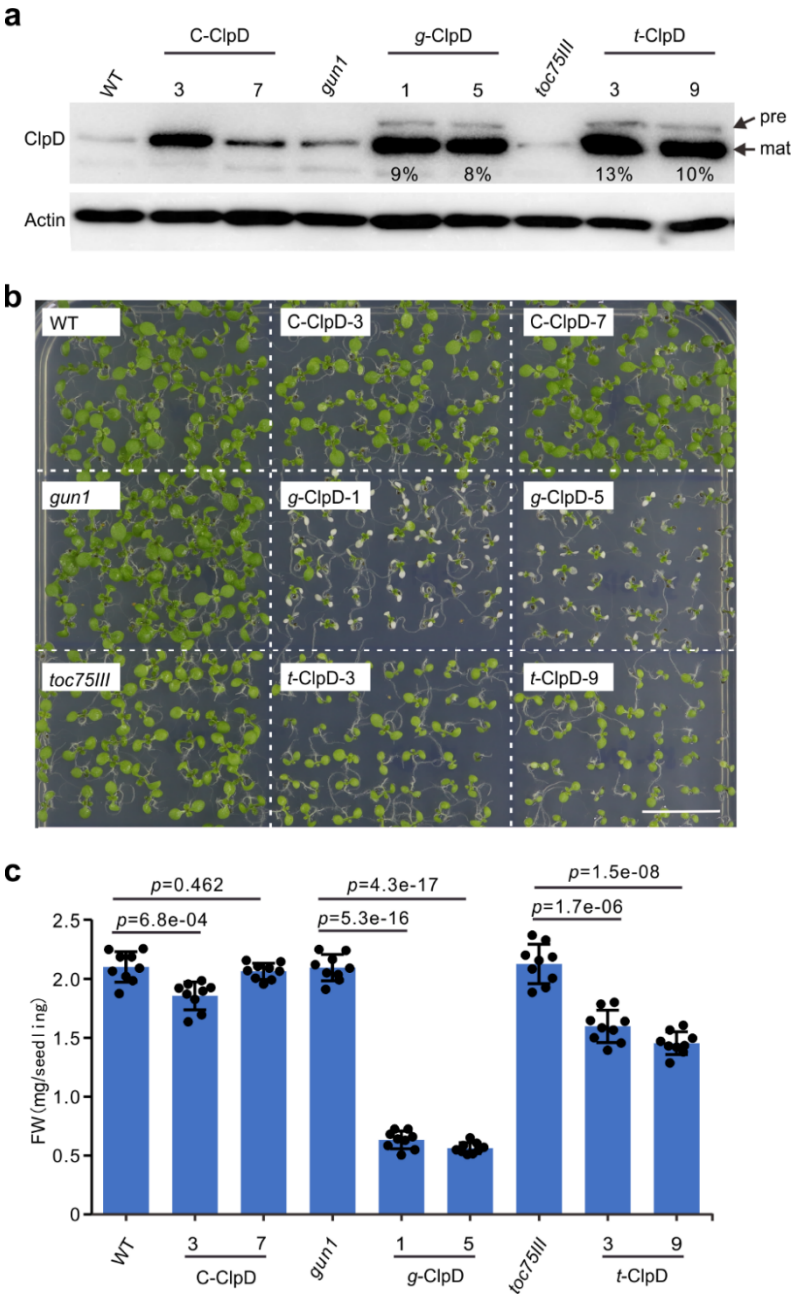

Supplementary Fig. 3 | Precursor accumulation results in retarded seedling growth.

a PreClpD accumulates in transgenic lines overexpressing ClpD in the *gun1* (*g*-ClpD) or *toc75III* (*t*-ClpD) background, but not in the WT (C-ClpD) background. Whole seedlings were used for analyses. Actin served as loading control. pre, preClpD; mat, mature ClpD. The numbers below the ClpD immunoblot represent the accumulation of preClpD relative to mature ClpD (in %). **b** Images of 8-d-old seedlings of the different genotypes analyzed in **a**. Scale bar, 1 cm. **c** Fresh weight measurements of the seedlings shown in **b**. Data are means ± s.d. ($n = 9$ biological replicates, each replicate represents the average of 10 seedlings). A two-tailed Student's *t*-tests were performed to determine the significance of differences.

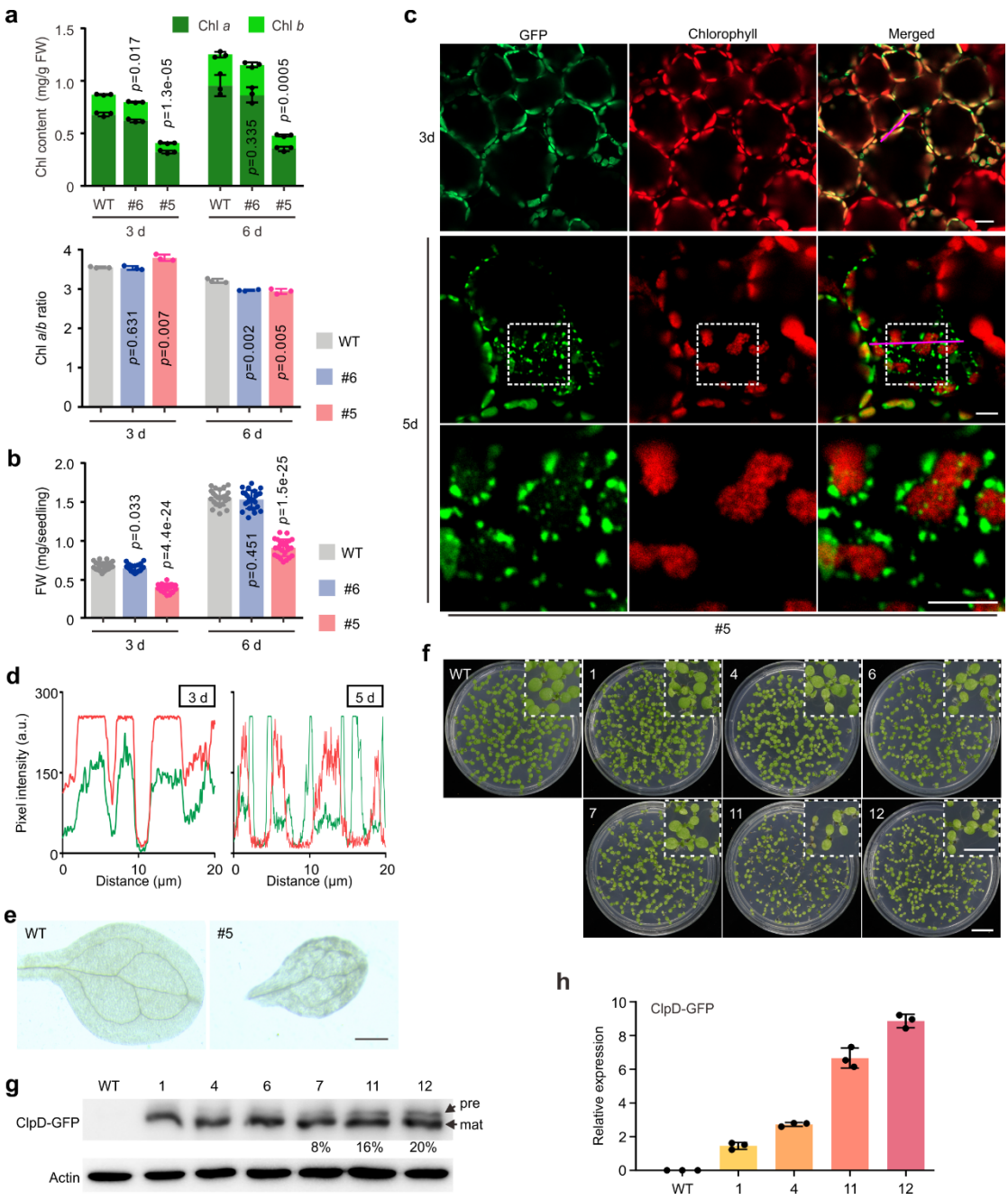

Supplementary Fig. 4 | Characterization of preClpD-GFP accumulation lines in the WT background.

a Chlorophyll (Chl) contents and Chl a/b ratios of 3-d-old and 6-d-old WT and constitutive ClpD-GFP overexpression lines under the WT background (#6 and #5). **b** Fresh weight measurements. In **a** and **b**, the data are means ± s.d. ($n = 3$ and 24 biological replicates in **a** and **b**, respectively. For fresh weight measurements, each replicate represents the average of 10 seedlings). Two-tailed Student's *t*-tests were performed to determine the significance of differences between genotypes. **c** PreClpD-GFP granules are closely distributed with the chloroplasts in the cotyledons of 5-d-old ClpD-GFP line #5 seedlings. The boxed areas were magnified and are shown below.

Scale bars, 10 μm. **d** Fluorescence intensity plots along the magenta lines shown in **c**. **e** Increased H_2O_2 accumulation in the cotyledons of 6-d-old seedlings of ClpD-GFP line #5 shown by 3,3'-diaminobenzidine (DAB) staining. Scale bar, 0.5 mm. **f** Phenotype segregation of the progeny of homozygous ClpD-GFP line #5. Although the line #5 is a homozygous line with single T-DNA insertion, the offsprings segregated as green and pale-green lines. Scale bars, 1 cm, and 0.5 cm for the enlarged insets. **g** Immunoblot showing the correlation of the retarded growth and pale-green phenotype in the offspring of ClpD-GFP line #5 (**f;** 11 and 12) with precursor accumulation. The numbers below the ClpD-GFP immunoblot represent the accumulation of preClpD-GFP relative to mature ClpD-GFP (in %). Actin served as loading control. pre, preClpD-GFP; mat, mature ClpD-GFP. **h** RT-qPCR analyses showing the expression of *ClpD-GFP* in the segregated green and chlorosis offspring of ClpD-GFP line #5. The primer pair that located in the GFP coding region was used. The relative expression of *ClpD-GFP* was compared to the Actin 7 gene in each sample and plotted. Data are means ± s.d. ($n = 3$ biological replicates). In **g** and **h**, whole seedling of 6-d-old were harvested for analyses.

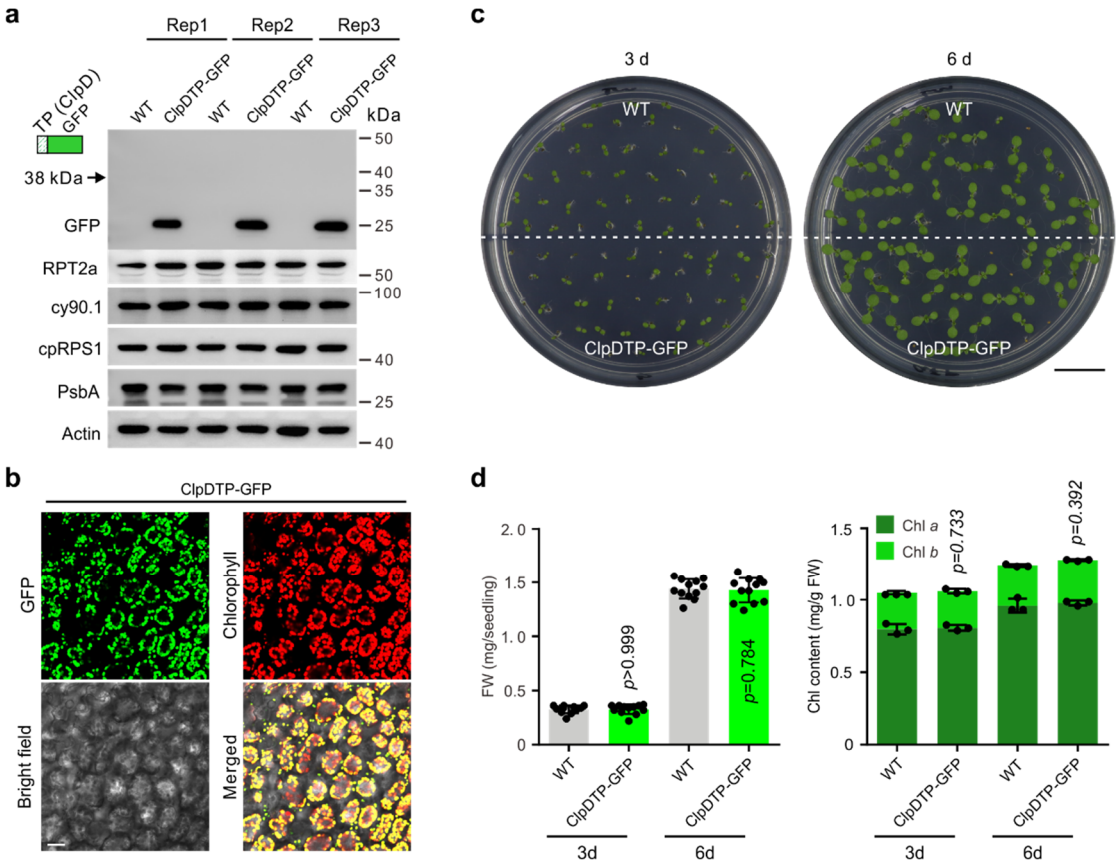

Supplementary Fig. 5 | The ClpDTP-GFP line shows no visible differences with the WT.

a The ClpDTP-GFP line[1] does not accumulate GFP precursor (~38 kDa) under normal growth conditions. The accumulation of 26S proteasome subunit RPT2a, cytosolic HSP90.1 (cy90.1), chloroplastic RPS1 (cpRPS1), and the PSII subunit PsbA was also analyzed. Whole seedling of 6-d-old were harvested for analyses. Actin served as loading control. **b** GFP signal was well colocalized with chlorophyll autofluorescence signal in the ClpDTP-GFP line. Seven-d-old seedlings were used for analysis. Scale bar, 20 μm. **c,d** The growth phenotype (**c**), fresh weight and chlorophyll content (**d**) of the WT and ClpDTP-GFP line at day 3 and 6. In **c**, scale bar, 1 cm. In **d**, Data are means ± s.d. (n = 12 for fresh weight, n=3 for chlorophyll content measurements). Two-tailed Student's t-tests were performed to determine the significance of differences between the WT and ClpDTP-GFP line.

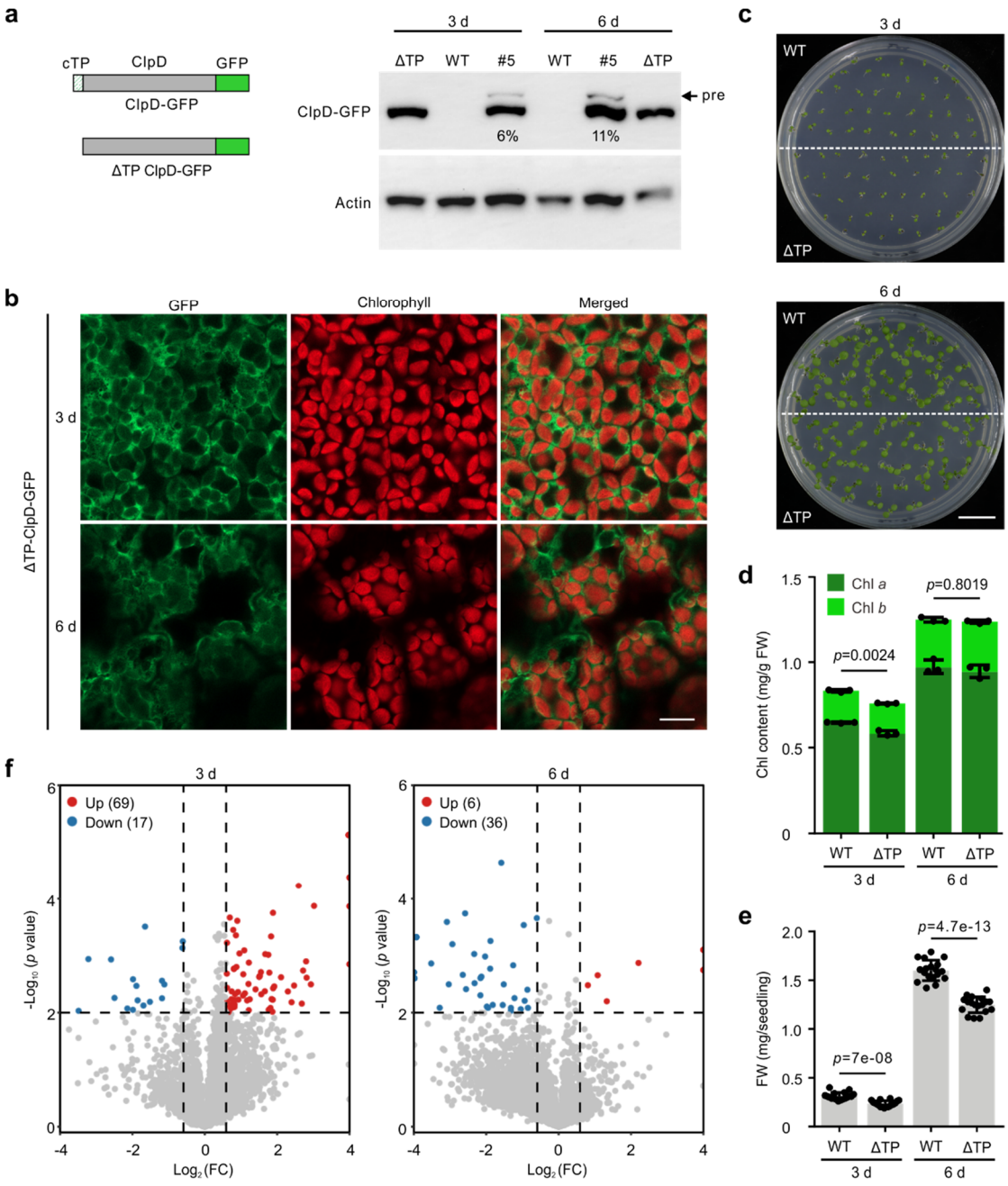

Supplementary Fig. 6 | Characterization of the ΔTP-ClpD-GFP overexpression line.

a Schematic representation of full-length ClpD (with cTP) and ΔTP-ClpD (without cTP) expressed as C-terminal GFP fusion proteins, and immunoblot analysis showing ClpD-GFP accumulation in 6-d-old ΔTP-ClpD-GFP (ΔTP) and ClpD-GFP line #5 (#5) seedlings. Whole seedlings were harvested for analyses. The WT was loaded as a control. The numbers below the ClpD-GFP immunoblot represent the accumulation of preClpD-GFP relative to mature ClpD-GFP (in %). Actin served as loading control. **b** Diffuse distribution of ΔTP-ClpD-GFP in the cytosol in cotyledons of 3-d-old and 6-d-old plants. Scale bar, 10 μm. **c** 3-d-old and 6-d-old seedlings of the WT and a

representative ΔTP-ClpD-GFP line. Scale bar, 1 cm. **d** Chlorophyll content measurements of 6-d-old WT and ΔTP-ClpD-GFP seedlings. Data are means ± s.d. (*n*=3 biological independent replicates). **e** Fresh weight measurements of 6-d-old seedlings. Data are means ± s.d. ($n = 18$ biological replicates, each replicate is an average of 10 seedlings). In **d** and **e**, two-tailed Student's *t*-tests were performed to determine the significance of differences between the WT and ΔTP-ClpD-GFP line. **f** Volcano plots showing the differentially expressed proteins of the 3-d-old or 6-d-old ΔTP-ClpD-GFP line in comparison to the WT.

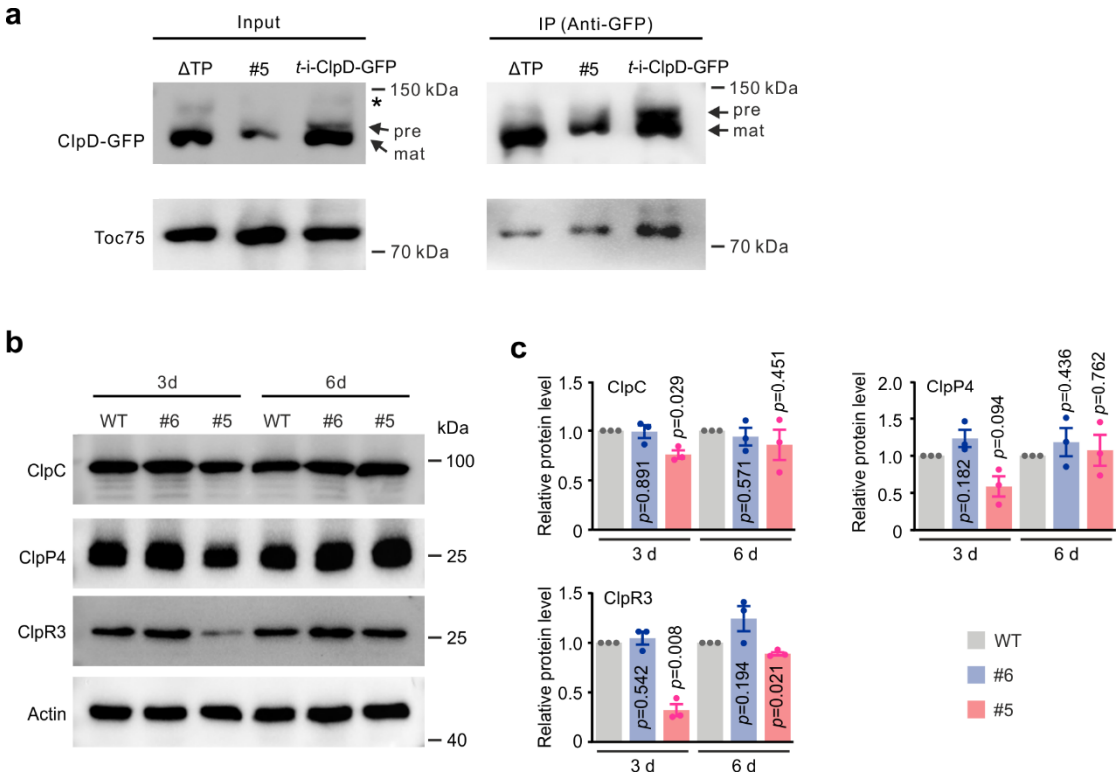

Supplementary Fig. 7 | Co-IP of ClpD-GFP in different genotypes and accumulation of the Clp protease subunits in the WT, ClpD-GFP line #6 and #5. **a** Co-IP of ClpD-GFP in ΔTP-ClpD-GFP (ΔTP), ClpD-GFP line #5 (#5), and *t*-i-ClpD-GFP lines. Note, the copurification of the Toc75 is corelated with the preClpD-GFP accumulation. For ΔTP-ClpD-GFP and ClpD-GFP line #5, total proteins were extracted from the whole seedlings of 5-d-old plants. For *t*-i-ClpD-GFP, 6-d-old seedlings were induced for another 4 days and the true leaves were harvested for total protein extraction and co-IP. **b,c** Immunoblot analyses of ClpC, ClpP4, ClpR3 in the seedlings from different genotypes at day 3 and day 6 (**b**) and the quantification from three biological replicates (**c**). Whole seedlings were harvested for analyses. Actin served as loading control. Data are means ± s.e. (n=3). Two-tailed Student's t-tests were performed to determine the significance of differences between the WT and transgenic lines.

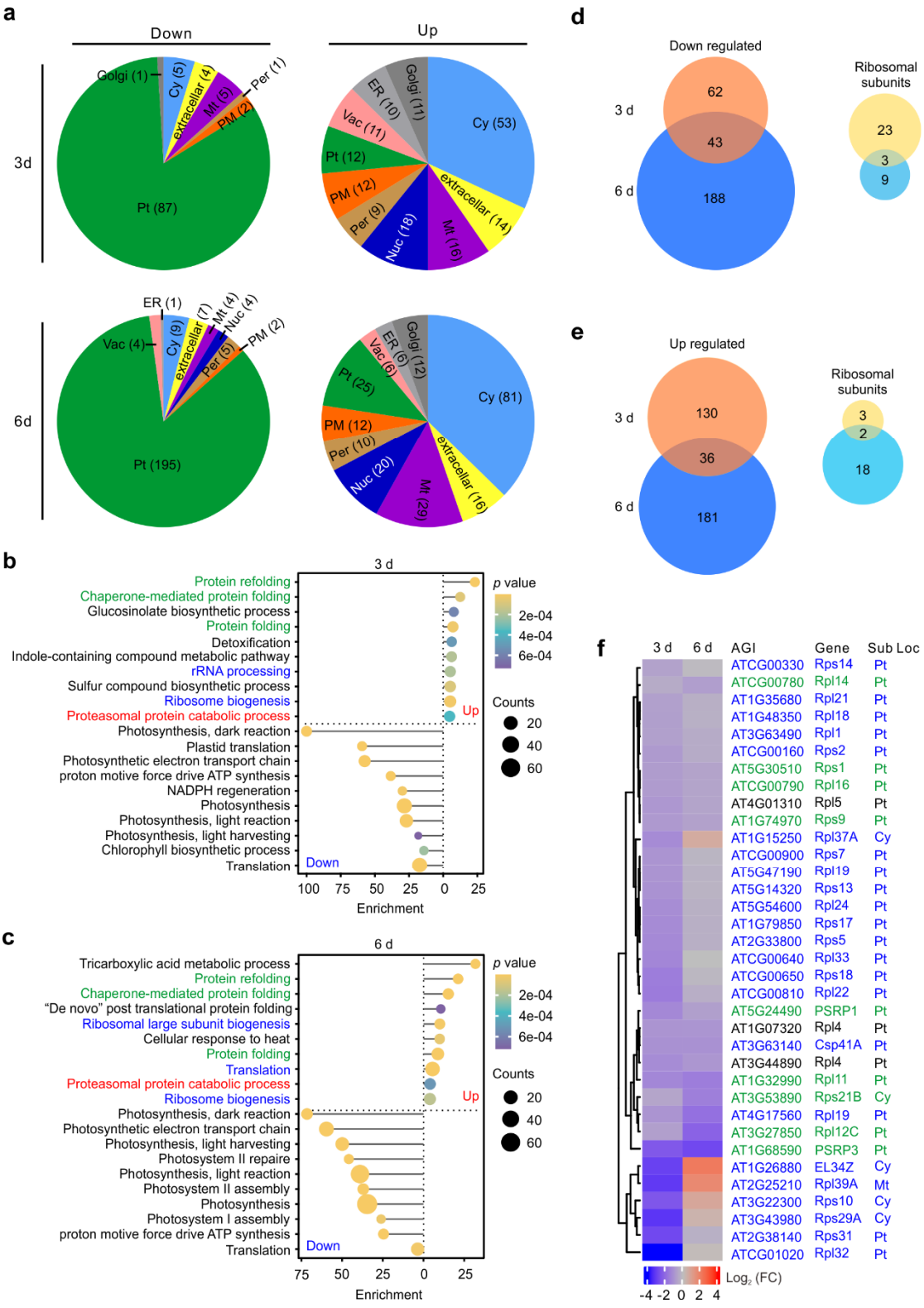

Supplementary Fig. 8 | Proteomic analyses of the 3-d-old and 6-d-old WT and line #5 plants.

a Subcellular localization of differentially expressed proteins. The numbers of differentially expressed proteins are indicated. Cy, cytosol; Mt, mitochondrion, Nuc, nucleus; Per, peroxisome; PM, plasma membrane; Pt, plastid; Vac, vacuole; ER,

endoplasmic reticulum; Golgi, Golgi apparatus. **b,c** GO term enrichment analysis of differentially expressed proteins in 3-d-old (**b**) and 6-d-old (**c**) ClpD-GFP line #5 seedlings compared to the WT. Significantly enriched GO terms were identified by Fisher's exact test with enrichment >3-fold and using FDR (<0.05) for multiple testing corrections. **d,e** Venn diagrams demonstrating the overlap of downregulated (**d**) or upregulated (**e**) proteins between the 3 d and 6 d timepoints. The comparison of differentially expressed ribosomal proteins is shown on the right. **f** Hierarchical clustering heatmap showing the 35 significantly downregulated ribosomal proteins. The 23 ribosomal proteins that were downregulated only at day 3 are colored in blue, and the 9 proteins that were significantly downregulated only at day 6 are colored in green. In **a** and **f**, the subcellular protein localization was annotated according to the SUBAcon localization of SUBA5 (http://suba.live).

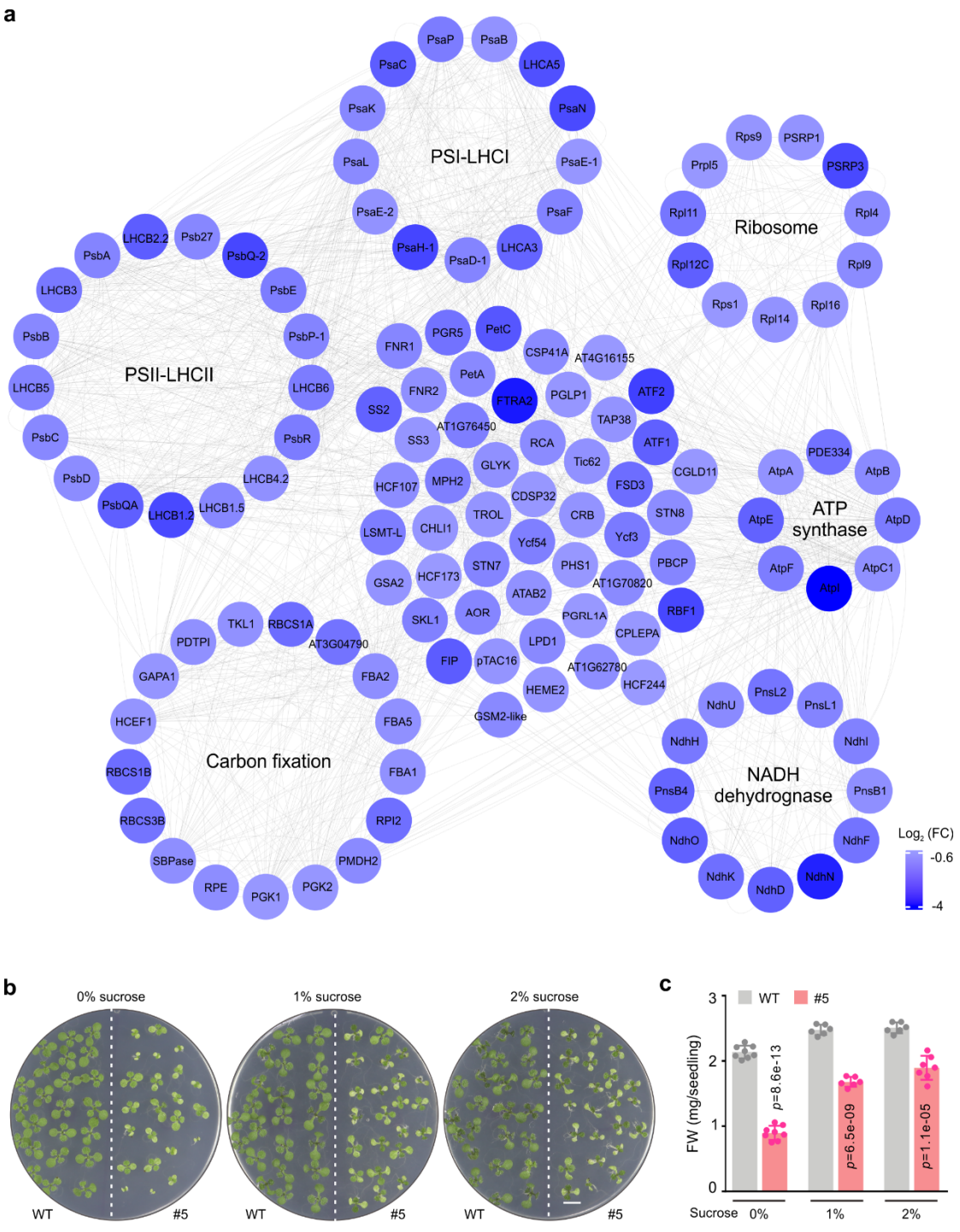

Supplementary Fig. 9 | Protein interaction network of downregulated proteins at day 6.

a Protein interaction network of downregulated proteins (ClpD-GFP line #5 compared to the WT) belonging to different complexes involved in photosynthetic light reactions, carbon fixation, and chloroplast ribosomes. The interaction network (including physical and functional interactions) was generated by STRING[2] and visualized by Cytoscape[3]. **b,c** Sucrose can partially rescue the decreased fresh-weight phenotype of ClpD-GFP line #5. Representative images (**b**) and quantification of the fresh weight of 8-d-old

plants are shown. In **c**, data are means ± s.d. (n = 6-8 biological replicates, each replicate is an average of 10 seedlings). Two-tailed Student's t-tests were performed to determine the significance of differences between the WT and ClpD-GFP line #5.

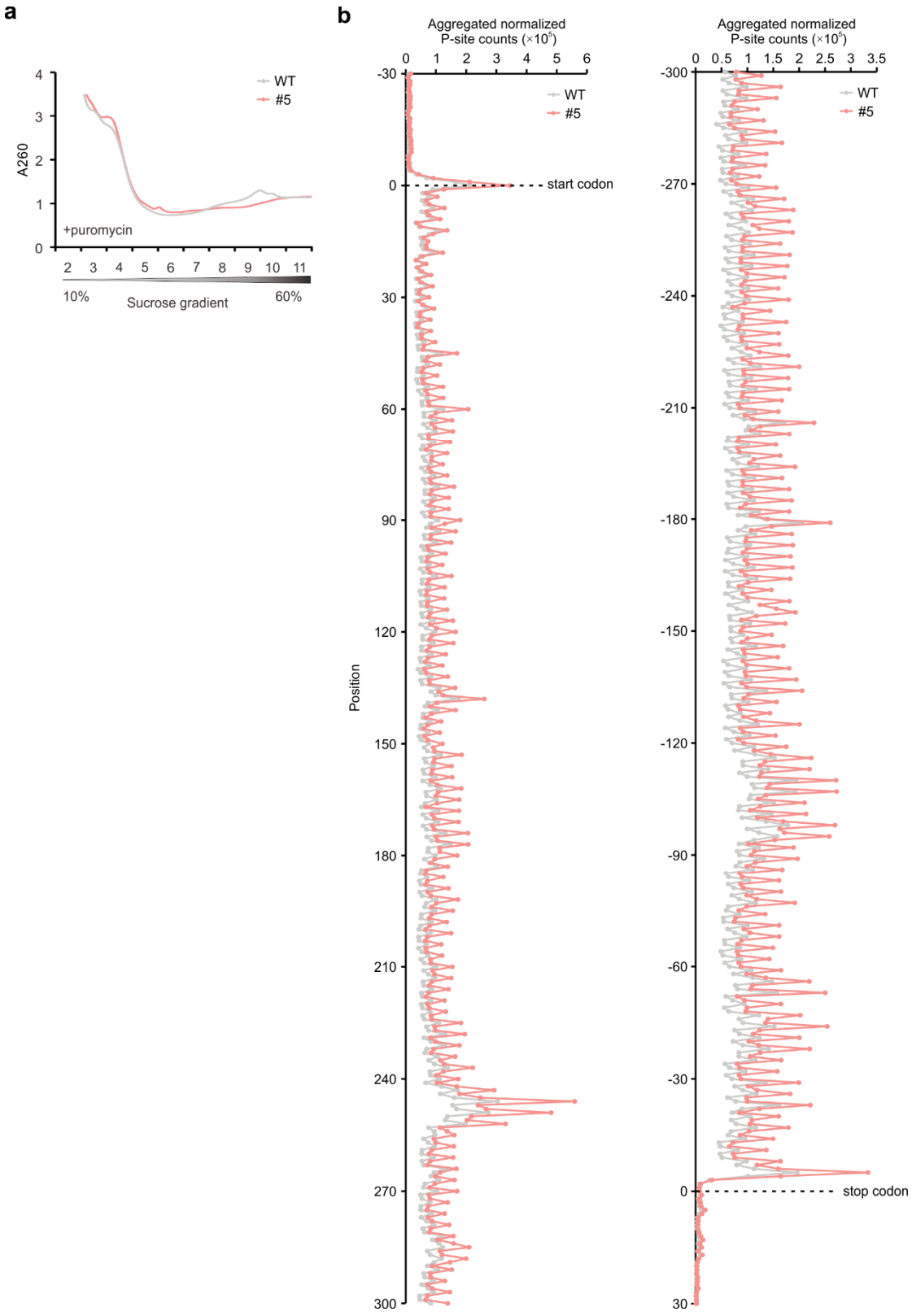

Supplementary Fig. 10 | Puromycin controls for the polysome profile analysis and genome-wide aggregated normalized P-site counts in the WT and ClpD-GFP line #5 from Ribo-seq data.

a Puromycin controls for the polysome profile analysis of the WT and ClpD-GFP line

#5 (cf. Fig. 3g). **b** Genome-wide aggregated normalized P-site counts in the WT and ClpD-GFP line #5 from Ribo-seq data. The regions 30 nt upstream and 300 nt downstream of the start codon, and 30 nt downstream and 300 nt upstream of the stop codon are shown (cf. Fig. 3h).

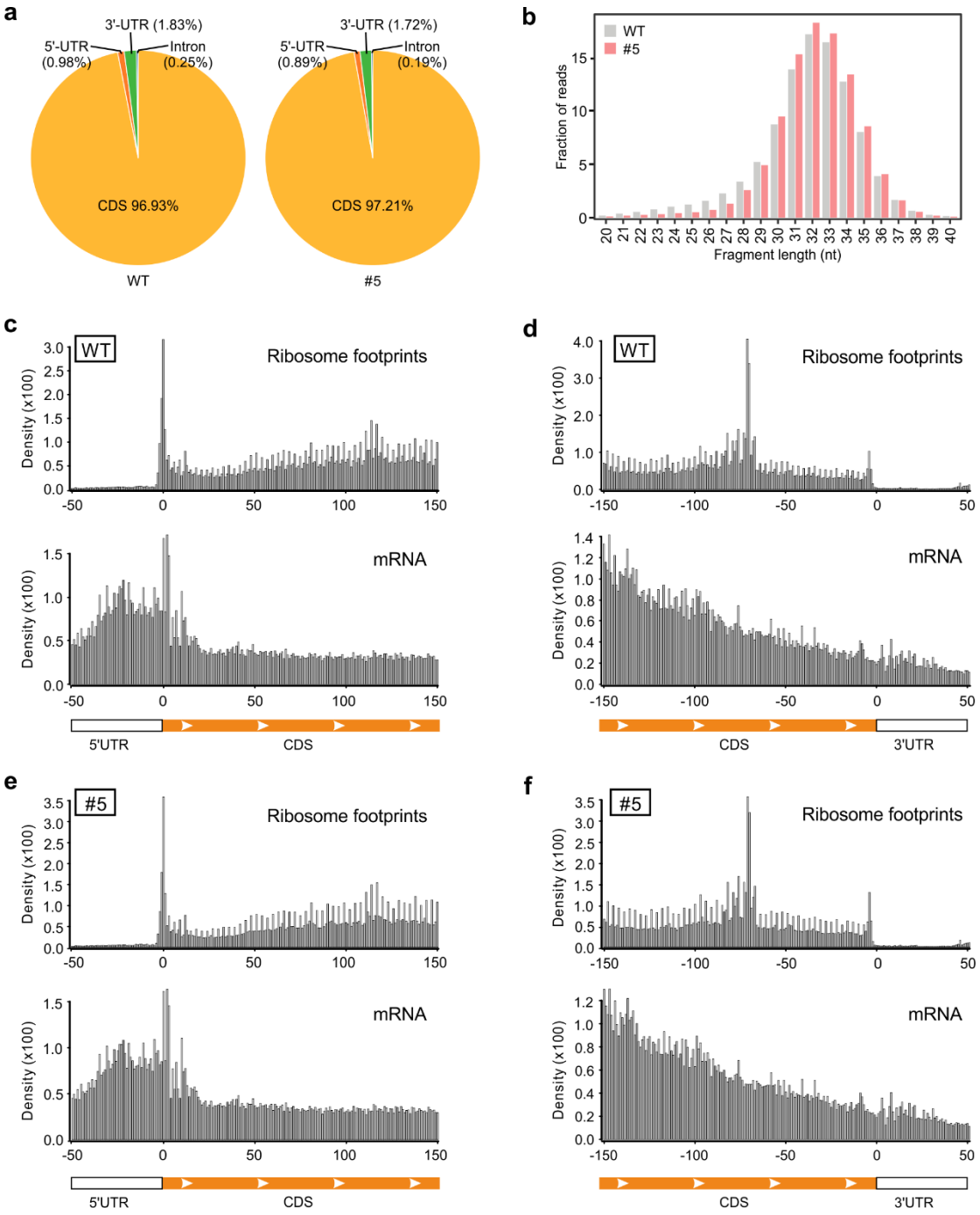

Supplementary Fig. 11 | Generation of high-quality Ribo-seq and RNA-seq libraries.

a Distribution of ribosome footprints across all annotated genes. Over 96% of ribosome footprints are located in CDS regions. UTR, untranslated region. **b** Distribution of read lengths in ribo-seq data. **c-f** Distribution of the ribosome footprint and mRNA reads for the WT (**c,d**) and ClpD-GFP line #5 (**e,f**) near the start codons and stop codons of all CDSs. As expected, strong 3-nt periodicity can only be seen in the Ribo-seq data.

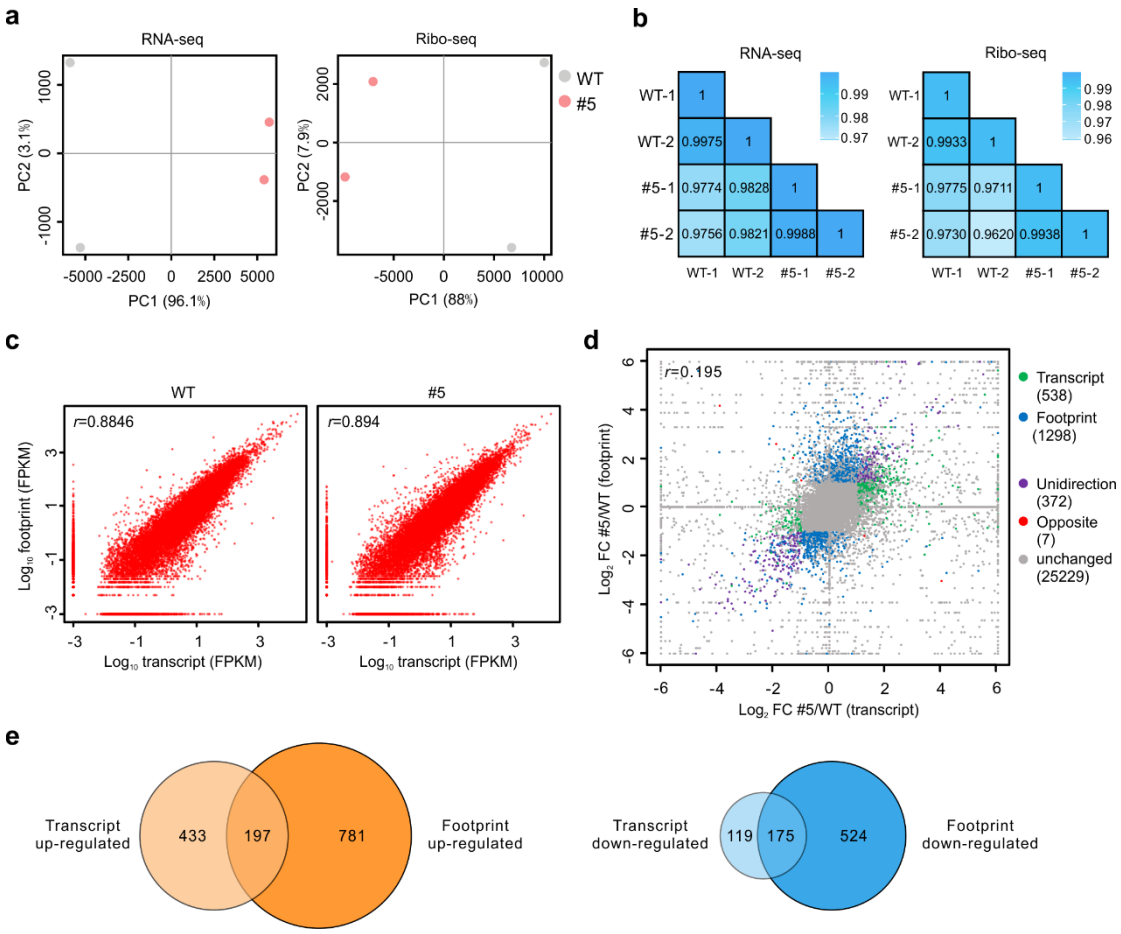

Supplementary Fig. 12 | Principal component analysis and correlation analysis of RNA-seq and Ribo-seq samples.

a Principal component analysis (PCA) of RNA-seq and Ribo-seq samples. **b** Pearson's correlation coefficients of gene expression profiles of transcripts and footprints for two biological replicates. **c** Extent of correlation between the abundance of transcripts and footprints of all genes in the WT and ClpD-GFP line #5. Pearson's correlation coefficients (*r*) are shown. **d** Extent of correlation between transcriptome changes and translatome changes in ClpD-GFP line #5 compared to WT. The Pearson's correlation coefficient (*r*) is shown. The differentially expression genes that only change at the transcript level or footprint level are colored in green or blue, respectively. The differentially expressed genes that change at both transcript and footprint levels with a unidirection or opposite direction are colored with purple or red, respectively. **e** Overlap of differentially expressed genes between the transcript level and the footprint level for upregulated and downregulated genes.

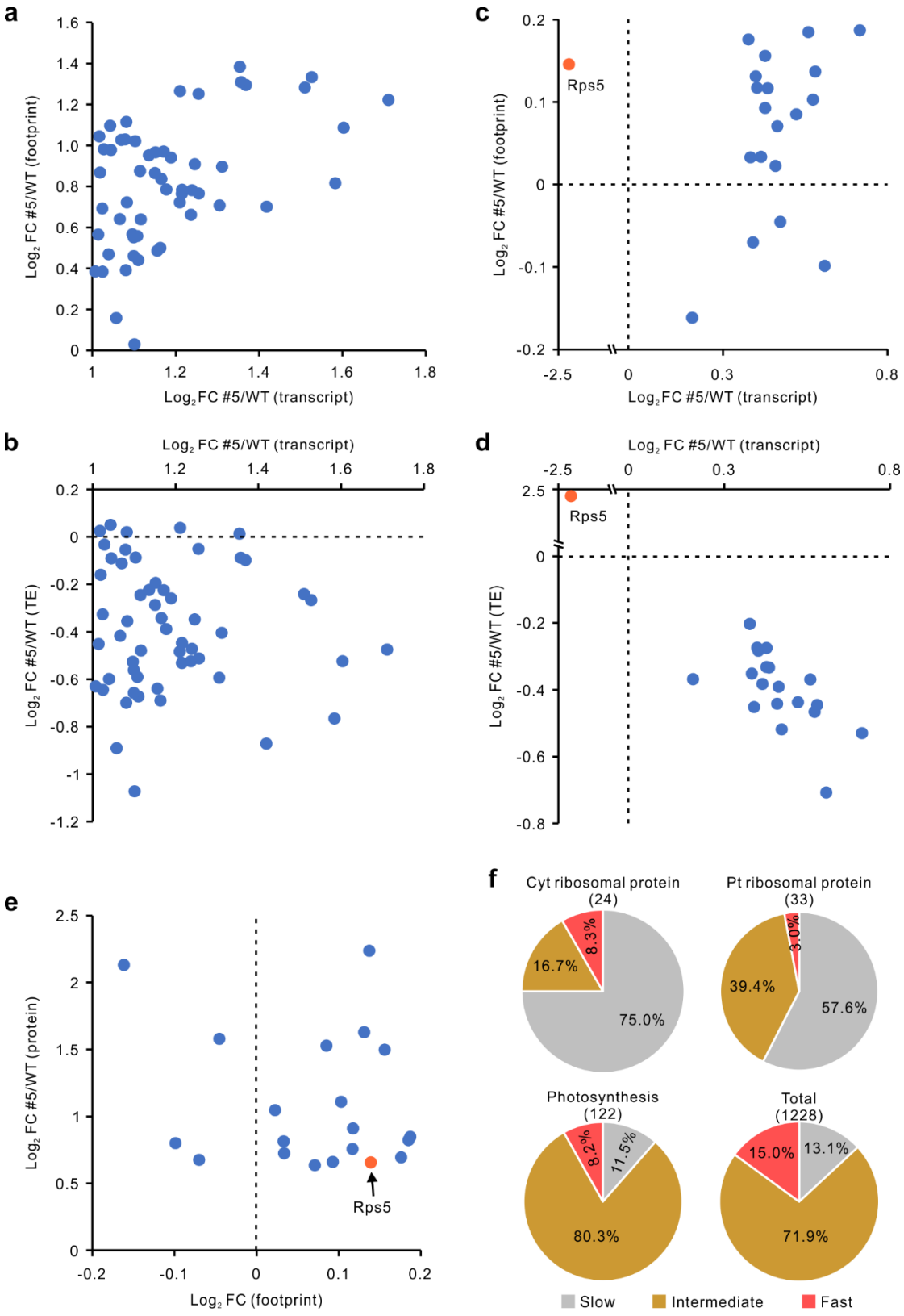

Supplementary Fig. 13 | Comparison of transcriptional and translational changes of differentially expressed genes involved in ribosome biogenesis or encoding cytosolic ribosomal proteins.

a,b Scatter plots illustrating the correlation between the fold change (FC) of transcript

and the FC of footprint (translation output; **a**) and between the FC of transcript and the FC of TE (**b**) for the transcriptionally upregulated genes enriched in GO terms related to ribosome biogenesis and rRNA processing/maturation (cf. Supplementary Data 6). **c-e** Scatter plots showing the correlation between the FC of transcript and the FC of footprint (**c**), between the FC of transcript and the FC of TE (**d**), and between the FC of footprint and the FC of protein (**e**) for cytosolic ribosomal proteins with increased protein abundance in 6-d-old ClpD-GFP line #5 seedlings (cf. Fig. 3d and Supplementary Data 6). **f** Venn diagram showing the percentages of proteins with slow, intermediate, or fast degradation rates. Cytosolic (Cyt) and plastid (Pt) ribosomal proteins, proteins related to photosynthesis, and all proteins determined by ^{15}N progressive labeling in a previous study[4] (cf. Supplementary Data 7) are represented by the four pie charts.

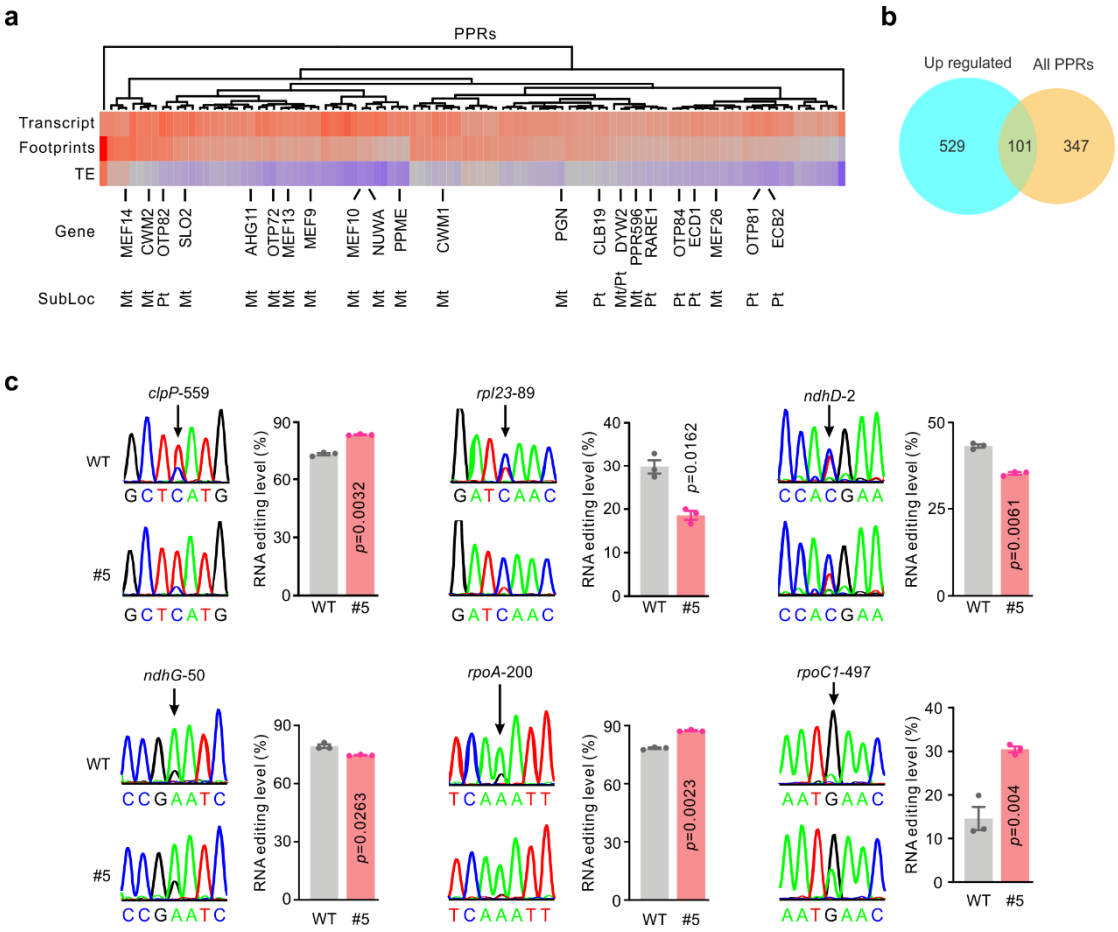

Supplementary Fig. 14 | Representative chloroplast RNA editing profiles of 6-d-old ClpD-GFP line #5 seedlings in comparison to the WT.

a Heatmap representation of the transcriptionally upregulated PPR genes and their changes at the footprint and TE levels. The gene names of representative PPRs reported to be involved in organellar RNA editing are indicated according to the plant editosome database[5]. **b** Venn diagram illustrating the 101 transcriptionally upregulated PPR genes in 6-d-old ClpD-GFP line #5 seedlings, which account for ~1/4 of the total PPRs in Arabidopsis[6]. **c** RNA editing profiles of 6 selected chloroplast RNA sites in 6-d-old WT and ClpD-GFP line #5 plants. The editing sites are indicated by arrows. Data are means ± s.e. (n=3). Two-tailed Student's t-tests were performed to determine the significance of differences between genotypes.

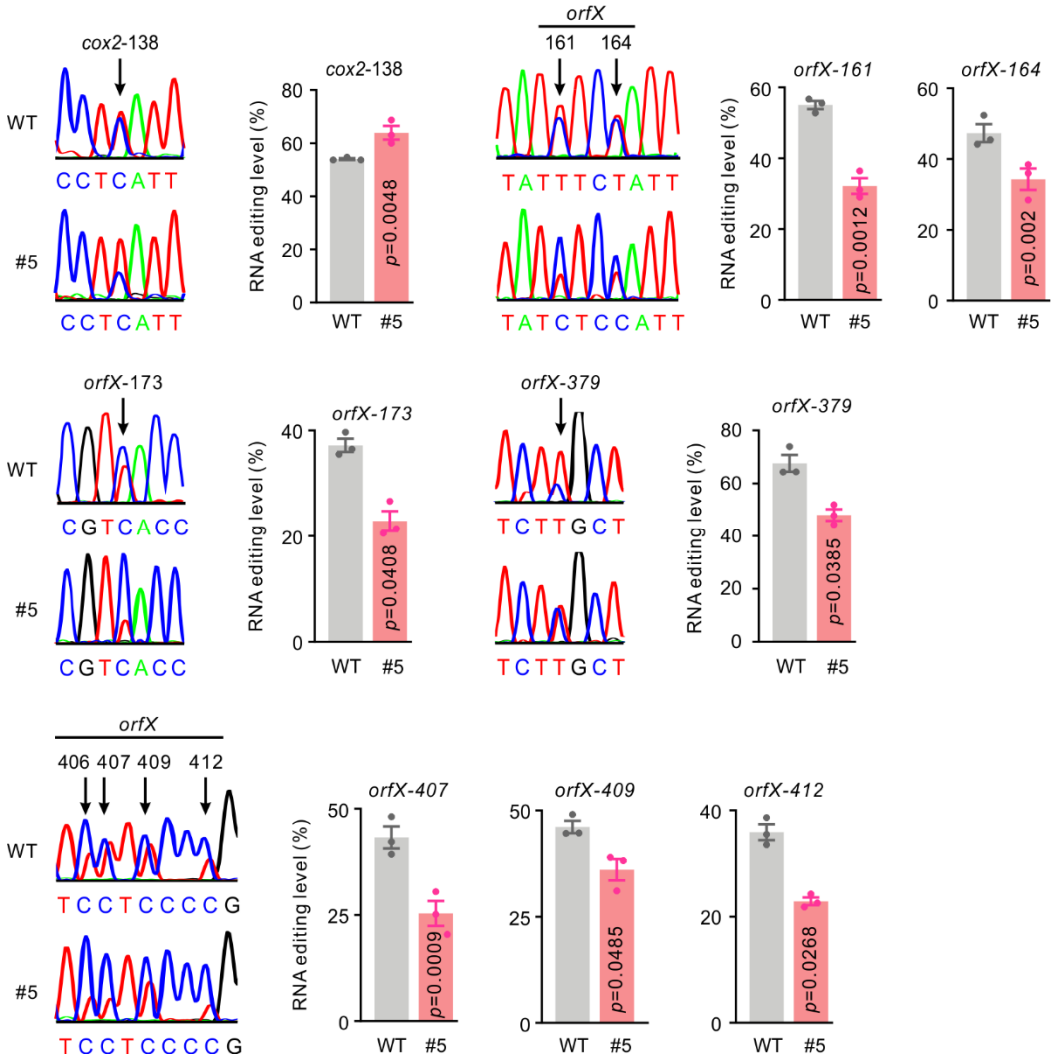

Supplementary Fig. 15 | Representative mitochondrial RNA editing profiles in 6-d-old ClpD-GFP line #5 seedlings in comparison to the WT.

The editing profiles of 8 editing sites from the *cox2 and orfX* genes were analyzed. The editing sites are indicated by arrows. Data are means ± s.e. (n=3). Two-tailed Student's t-tests were performed to determine the significance of differences between genotypes.

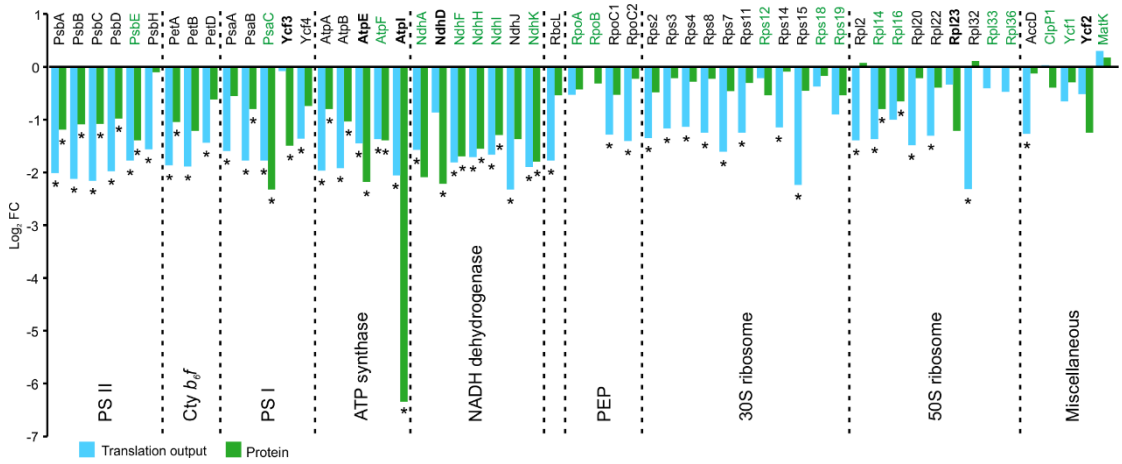

Supplementary Fig. 16 | Comparison of the changes of chloroplast-encoded genes at the translation output and protein levels.

Significant changes at the translation output (footprint) level or protein level are marked with asterisks. Genes with a protein FC (ClpD-GFP line #5/WT) over translation output FC (ClpD-GFP line #5/WT) of less than 1.5-fold are marked in green. Genes with a protein FC (ClpD-GFP line #5/WT) decrease larger than the translation output FC (ClpD-GFP line #5/WT) decrease are in bold.

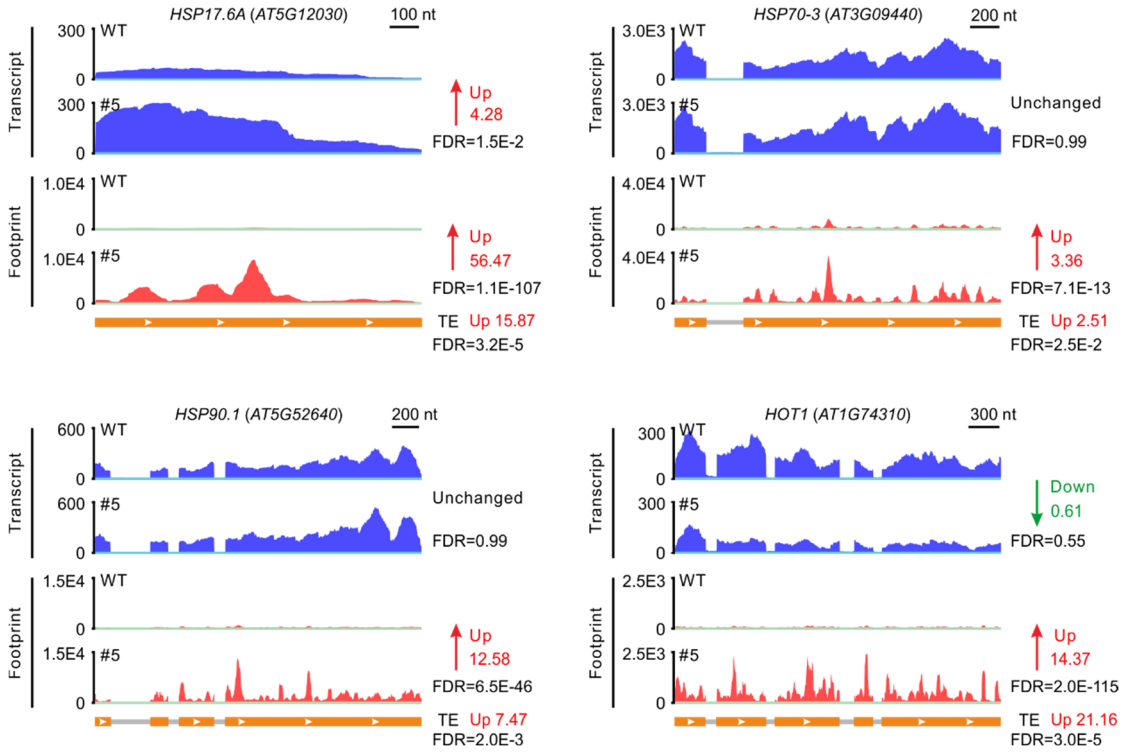

Supplementary Fig. 17 | Normalized distribution of RNA-seq and Ribo-seq reads over selected *HSP* genes in the WT and ClpD-GFP line #5.

The fold change and the associated FDR at the transcript, footprint, and TE levels are shown.

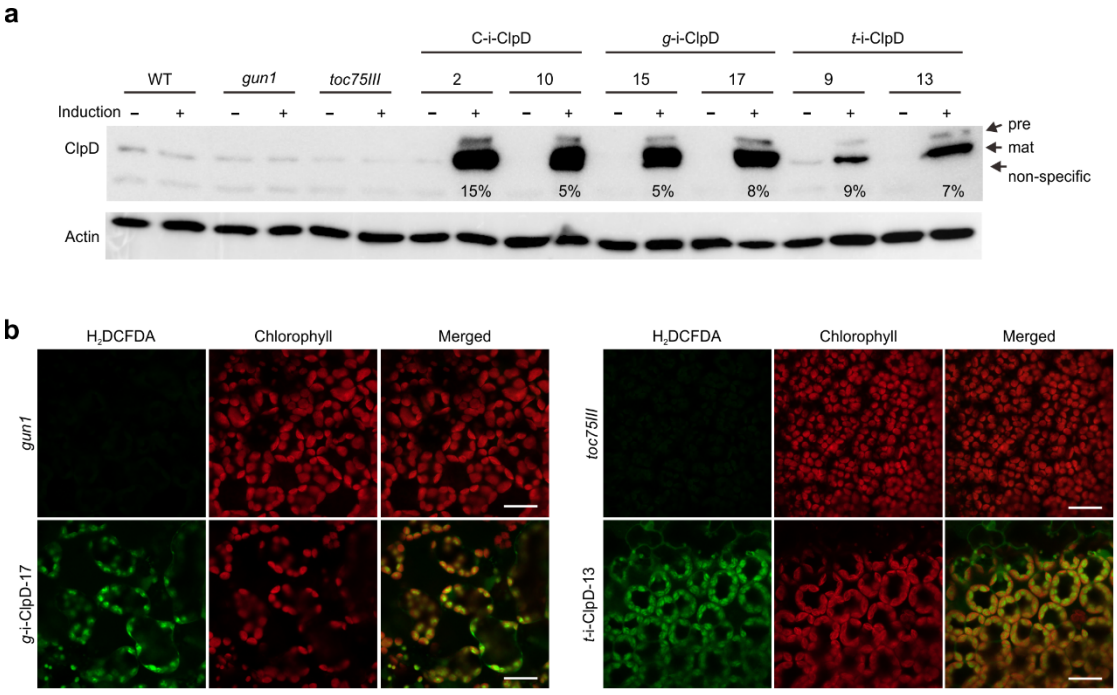

Supplementary Fig. 18 | Precursor accumulation induces a ROS burst in chloroplasts.

a Accumulation of (pre)ClpD at 12 h of induction in inducible ClpD expression lines in the WT (C-i-ClpD), *gun1* (*g*-i-ClpD), or *toc75III* (*t*-i-ClpD) background. Six-d-old seedlings were induced for another 12 h and whole seedlings were harvested for analyses. Untransformed WT, *gun1*, and *toc75III* were included as controls. Actin served as a loading control. The numbers below the ClpD immunoblot represent the accumulation of preClpD relative to the mature ClpD (in %). pre, preClpD; mat, mature ClpD. **b** ROS burst in the chloroplasts of the *g*-i-ClpD-17 and *t*-i-ClpD-13 lines at 12 h of induction. The untransformed *gun1* and *toc75III* parental lines were included as controls. Newly emerged true leaves from 6-d-old seedlings were stained with the H_2DCFDA fluorescent dye for ROS visualization. Scale bars, 20 μm.

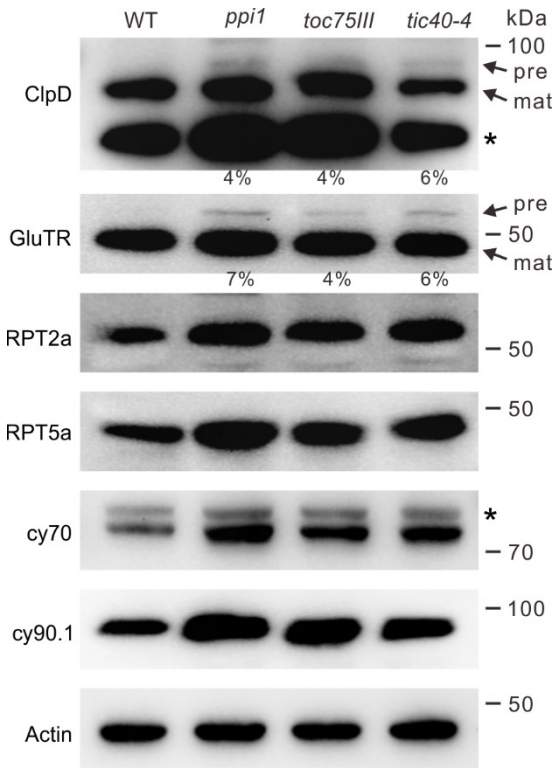

Supplementary Fig. 19 | Accumulation of precursor proteins in protein import-related mutants.

The precursors of ClpD and GluTR were observed in *ppi1*, *toc75III*, and *tic40-4* mutants. Meanwhile, the protein levels of 26S proteasome subunits RPT2a and RPT5a, and cytosolic chaperones HSP70 (cy70) and HSP90.1 (cy90.1) increased in these mutants. The numbers below the ClpD and GluTR immunoblots represent the accumulation of precursors relative to the mature proteins (in %). The newly emerged true leaves from 7-d-old seedlings were used for analyses. The experiments were repeated independently with similar results. Asterisks indicate nonspecific crossreations of the antibodies. Actin served as loading control.

a

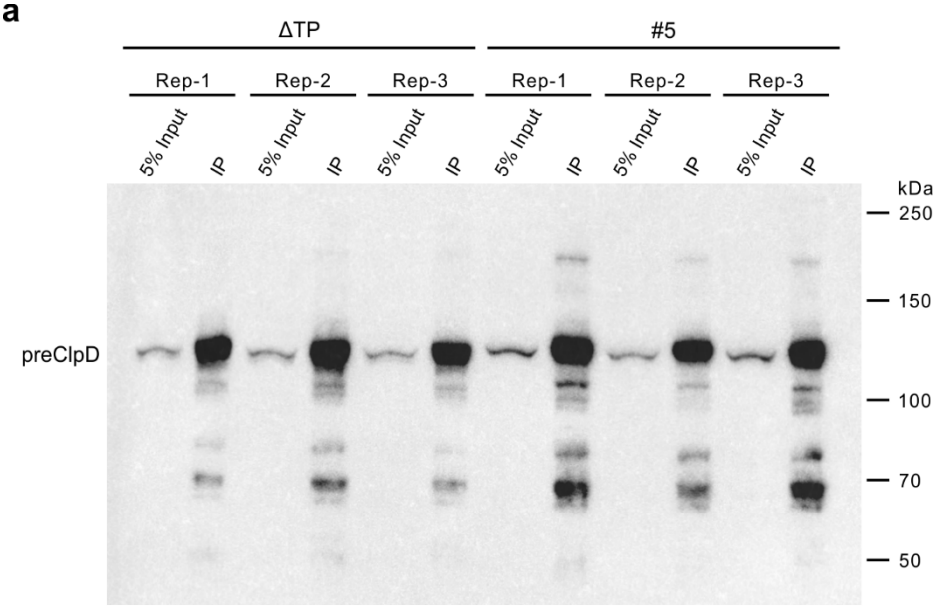

b

		ΔTP (P-TP intensity)			#5 (P-TP intensity)		
Protein	AGI	Rep-1	Rep-2	Rep-3	Rep-1	Rep-2	Rep-3
ClpD	AT5G51070	411140	0	0	48722100	202743000	454594000
ClpC1	AT5G50920	0	0	0	2017800	8963300	23103000
AOC2	AT3G25770	0	1473200	8932400	0	5068500	8201200
GLU1	AT5G04140	2737600	0	4771500	834870	3731600	5418900
LhcB1.3	AT1G29930	0	0	0	474880	2138300	4440400
AK1	AT5G13280	0	1121600	2728800	0	2286500	3464200
UCK1	AT5G40870	0	0	0	0	0	5409900

Supplementary Fig. 20 | Identification of preClpD-GFP associated proteins by co-IP and mass spectrometric analyses.

a Immunoblot analysis showing the three biological replicates of the co-IP of ΔTP-ClpD-GFP and ClpD-GFP line #5 that were used for mass spectrometric identification of preClpD-GFP associated proteins. Crude cytosolic fractions from 6-d-old ΔTP-ClpD-GFP and ClpD-GFP line #5 seedlings were isolated and incubated with anti-GFP magnetic beads. The blot was immunodetected with anti-GFP antibodies. **b** The P-TPs identified from the immunoprecipitates by mass spectrometry. The LFQ intensities of P-TPs identified are shown.

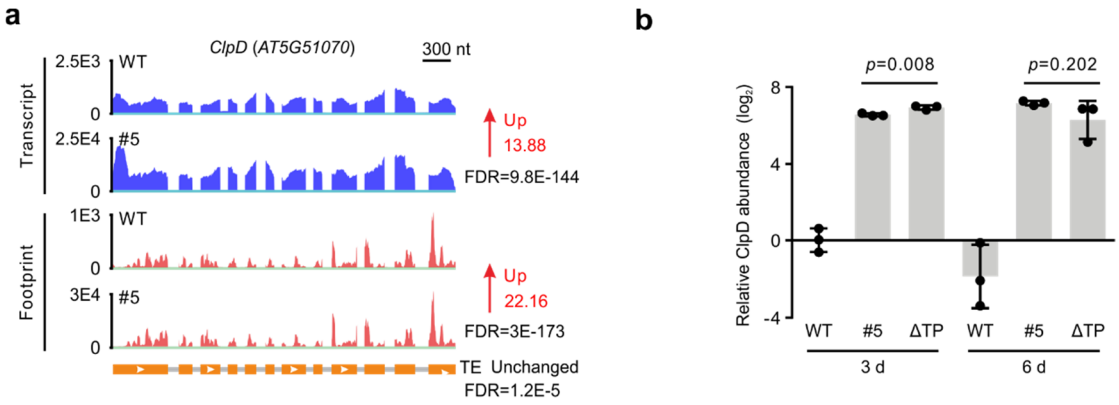

Supplementary Fig. 21 | Normalized distribution of RNA-seq and Ribo-seq reads over the *ClpD* gene, and ClpD protein abundance in different samples.

a Normalized distribution of RNA-seq and Ribo-seq reads over the *ClpD* gene. The fold change and the associated FDR at the transcript, footprint, and TE levels are shown. **b** ClpD protein abundance determined by mass spectrometry from three biological replicates. The relative ClpD protein abundance is compared to one replicate of the WT at day 3 (set as 1.0). Data are means ± s.d. (n=3). Two-tailed Student's t-tests were performed to determine the significance of differences between the ClpD-GFP line #5 and ΔTP-ClpD-GFP.

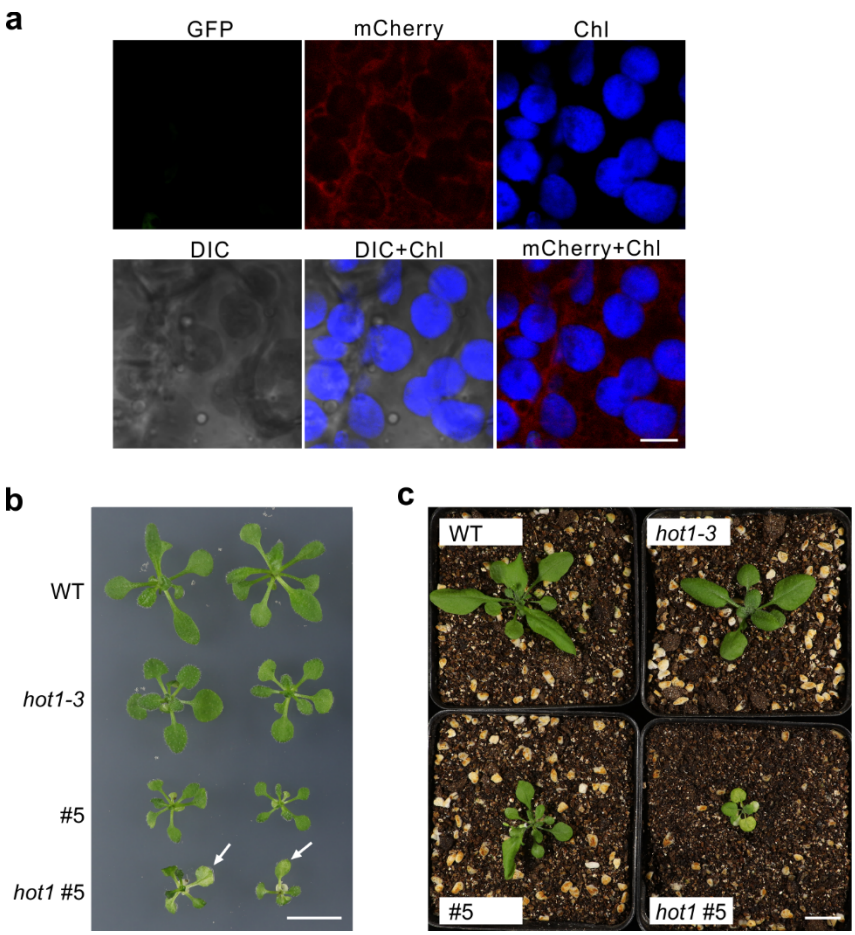

Supplementary Fig. 22 | Distribution of HOT1-mCherry in cells without preClpD-GFP granule accumulation and the growth phenotype of ClpD-GFP line #5 and *hot1* #5.

a, HOT1-mCherry defuse distributed in the cytosol in the cells without preClpD-GFP granule accumulation, in contrast, it forms granules in the cells with preClpD-GFP granule accumulation (Fig. 7f). The 5-d-old #5/HOT1-mCherry seedlings were used for analyses. Scale bar, 5 μm. Chl, Chlorophyll. **b,c** The WT, *hot1-3*, ClpD-GFP line #5, and *hot1* #5 (line #5 crossed into *hot1-3* background) were grown on half strength of MS medium for 16 days (**a**) or for 7 days and then planted in soil for another 21 days (**b**). Scale bars, 1 cm.

Supplementary Table 1. Transgenic lines used in this study.

Name	Background	Promoter	Type	Description	Generated by
C-i-ClpD	Col-0	alcA	Ethanol inducible	Inducible overexpression of ClpD in the Col-0 background	This study
g-i-ClpD	*gun1-101*	alcA	Ethanol inducible	Inducible overexpression of ClpD in the *gun1* background	This study
t-i-ClpD	*toc75III-3*	alcA	Ethanol inducible	Inducible overexpression of ClpD in the *toc75III* background	This study
C-i-ClpD-GFP	Col-0	alcA	Ethanol inducible	Inducible overexpression of ClpD-GFP in the Col-0 background	This study
g-i-ClpD-GFP	*gun1-101*	alcA	Ethanol inducible	Inducible overexpression of ClpD-GFP in the *gun1* background	This study
t-i-ClpD-GFP	*toc75III-3*	alcA	Ethanol inducible	Inducible overexpression of ClpD-GFP in the *toc75III* background	This study
C-ClpD	Col-0	CaMV 35S	Constitutive	Constitutive overexpression of ClpD in the Col-0 background	Wu et al.[1]
g-ClpD	*gun1-101*	CaMV 35S	Constitutive	Constitutive overexpression of ClpD in the *gun1* background	Wu et al.[1]
t-ClpD	*toc75III-3*	CaMV 35S	Constitutive	Constitutive overexpression of ClpD in the *toc75III* background	This study
ClpD-GFP lines (#5 and #6)	Col-0	CaMV 35S	Constitutive	Constitutive overexpression of ClpD-GFP in the Col-0 background	This study
#5/HOT1-mCherry	ClpD-GFP line #5	CaMV 35S	Constitutive	Constitutive expression of HOT1-mCherry in the ClpD-GFP line #5 background	This study
hot1 #5	ClpD-GFP line #5	CaMV 35S	Constitutive	Crossing the ClpD-GFP line #5 into *hot1-3* mutant background	This study
cpGFP *tic40-4*	*tic40-4*	CaMV 35S	Constitutive	cpGFP expression line (chloroplast-targeted GFP by RbcS TP) from Wu et al.[7] was crossed into *tic40-4* background	This study
ClpDTP-GFP	Col-0	CaMV 35S	Constitutive	Constitutive overexpression of ClpD TP (1-89AA) fused with GFP in the Col-0 background	Wu et al.[1]
ΔTP-ClpD-GFP	Col-0	CaMV 35S	Constitutive	Constitutive overexpression of ClpD-GFP without cTP (1-89AA) in the Col-0 background	This study

Supplementary Table 2. Sequencing read counts and mapping rates in RNA-seq and Ribo-seq experiments.

RNA-seq sequencing read counts and mapping rates						
Sample		Total Reads	Unmapped Reads	Unique Mapped Reads	Multiple Mapped reads	Mapping Ratio
WT	Rep1	43097562	394121 (0.91%)	41895276 (97.21%)	808165 (1.88%)	42703441 (99.09%)
	Rep2	45365756	421063 (0.93%)	44095546 (97.20%)	849147 (1.87%)	44944693 (99.07%)
ClpD-GFP #5	Rep1	48723210	842058 (1.73%)	46985065 (96.43%)	896087 (1.84%)	47881152 (98.27%)
	Rep2	47435358	635814 (1.34%)	45940229 (96.85%)	859315 (1.81%)	46799544 (98.66%

Ribo-seq sequencing read counts and mapping rates						
Sample		Total Reads	Unmapped Reads	Unique Mapped Reads	Multiple Mapped reads	Mapping Ratio
WT	Rep1	34057352	458578 (1.35%)	29494689 (86.60%)	4104085 (12.05%)	33598774(98.65%)
	Rep2	31496386	554531 (1.76%)	27023487 (85.80%)	3918368 (12.44%)	30941855(98.24%)
ClpD-GFP #5	Rep1	47244293	400185 (0.85%)	41989108 (88.88%)	4855000 (10.28%)	46844108(99.15%)
	Rep2	43681937	393547 (0.90%)	38858344 (88.96%)	4430046 (10.14%)	43288390(99.1%)

Supplementary Table 3. List of primers used in this study for genotyping, cloning, and qPCR analyses. Restriction sites used for cloning are underlined in the sequences.

Primers	AGI	Sequence (5'-3')	Description and usage
HSP17.4 -F	AT3G46230	TGAAGAGAAGAGTGACACATGG	Forward primer for qRT-PCR analysis for *HSP17.4*
HSP17.4 -R	AT3G46230	TCTCCATACTCGCCTTTACTTC	Reverse primer for qRT-PCR analysis for *HSP17.4*
HSP17.6A -F	AT5G12030	TTTTCAATCCTCGAAGACATGC	Forward primer for qRT-PCR analysis for *HSP17.6A*
HSP17.6A -R	AT5G12030	CTTGTTGTCCCTCTGTCTTTTG	Reverse primer for qRT-PCR analysis for *HSP17.6A*
HSP17.6C -F	AT1G53540	GTTCACAAACGCTAAAGTGGAT	Forward primer for qRT-PCR analysis for *HSP17.6C*
HSP17.6C -R	AT1G53540	GAAGTATGTTGCCATCCTCAAC	Reverse primer for qRT-PCR analysis for *HSP17.6C*
HSP18.5 -F	AT2G19310	CCCATCACCAGCTCTCTTTCTT	Forward primer for qRT-PCR analysis for *HSP18.5*
HSP18.5 -R	AT2G19310	CTACGAACGCAATCACTTCGTC	Reverse primer for qRT-PCR analysis for *HSP18.5*
HSP21 -F	AT4G27670	ACAACGCTTAACCATGGACG	Forward primer for qRT-PCR analysis for *HSP21*
HSP21 -R	AT4G27670	GGTGCACGAATCTCTGACAC	Reverse primer for qRT-PCR analysis for *HSP21*
HSP23.5- F	AT5G51440	TCTCTCTTCTTCCACCGTCG	Forward primer for qRT-PCR analysis for *HSP23.5*

HSP23.5- R	AT5G51440	ATGTGAGAAGAAATCGCCGC	Reverse primer for qRT-PCR analysis for *HSP23.5*
HSP23.6 -F	AT4G25200	GTGTTCTTCGTCCAGCTGTTTC	Forward primer for qRT-PCR analysis for *HSP23.6*
HSP23.6 -R	AT4G25200	GAGGAACAGAGCGGCGATATAA	Reverse primer for qRT-PCR analysis for *HSP23.6*
mtHSC70-1-F	AT4G37910	GGTCGAAGCCAATGGACAAA	Forward primer for qRT-PCR analysis for *mtHSC70-1*
mtHSC70-1-R	AT4G37910	TAGTGGCTTGTCTCTGTGCA	Reverse primer for qRT-PCR analysis for *mtHSC70-1*
HSP90C-F	AT2G04030	TGAAGACACCGGTAACCACA	Forward primer for qRT-PCR analysis for *HSP90C*
HSP90C-R	AT2G04030	TCCAAGAAAGGGGCAGACTT	Reverse primer for qRT-PCR analysis for *HSP90C*
GFP-F		GAGCTGAAGGGCATCGACTT	Forward primer for qRT-PCR analysis for *ClpD-GFP*
GFP-R		TTCTGCTTGTCGGCCATGAT	Reverse primer for qRT-PCR analysis for *ClpD-GFP*
Actin-qF	AT5G09810	CCGGTATTGTGCTCGATTCTG	Forward primer for qRT-PCR analysis for *ACTIN*
Actin-qR	AT5G09810	TTCCCGTTCTGCGGTAGTGG	Reverse primer for qRT-PCR analysis for *ACTIN*
hot1-3-F	AT1G74310	CAAGCTGCTCAGAAGTCACG	Forward primer for *hot1-3* T-DNA insertion mutant identification
hot1-3-R	AT1G74310	CTCCTCTCAAAGGCAGCATC	Reverse primer for *hot1-3* T-DNA insertion mutant identification
GUN1-F	At2G31400	TGCTACTAGAGGAGCTCAGGC	Forward primer for *gun1* T-DNA insertion

			mutant identification
GUN1-R	At2G31400	CCCTCAAAAGAACTTCAACCG	Reverse primer for *gun1* T-DNA insertion mutant identification
Toc75III-F	AT3G46740	TGCTTCAACAGCCGCAAACT	Forward primer for *toc75III* point mutation mutant identification
Toc75III-R	AT3G46740	TACGGACCACCGAGGACA	Reverse primer for *toc75III* point mutation mutant identification
clpP-559-F	ATCG00670	ATGATCCATCAACCCGCTAG	Forward primer for RNA editing analysis for site *clpP-559*
clpP-559-R	ATCG00670	TATTGAACCGCTACAAGATC	Reverse primer for RNA editing analysis for site *clpP-559*
ndhD-2-F	ATCG01050	GACTGTGTTGGTTGTAAGAGATGTG	Forward primer for RNA editing analysis for site *ndhD-2*
ndhD-2-R	ATCG01050	TCGATCCATTTATAATCTTCGGA	Reverse primer for RNA editing analysis for site *ndhD-2*
ndhG-50-F	ATCG01080	ATAATGGATTTGCCTGGACC	Forward primer for RNA editing analysis for site *ndhG-50*
ndhG-50-R	ATCG01080	CTTATTAAATCTTGCTCTAGAATCTGGTT	Reverse primer for RNA editing analysis for site *ndhG-50*
rpl23-89-F	ATCG00840	AATTCCTACTGGATGCACGC	Forward primer for RNA editing analysis for site *rpl23-89*
rpl23-89-R	ATCG00840	AAGAGGTGGAATAGAATAACCCG	Reverse primer for RNA editing analysis for site *rpl23-89*
rpoA-200-F	ATCG00740	CGGACACTACAGTGGAAGTG	Forward primer for RNA editing analysis for site *rpoA-200*

rpoA-200-R	ATCG00740	ATGAATACAGCATCGATAGG	Reverse primer for RNA editing analysis for site *rpoA-200*
rpoC1-497-F	ATCG00180	TTTTCTTTTGCTAGGCCCATAA	Forward primer for RNA editing analysis for site *rpoC1-497*
rpoC1-497-R	ATCG00180	TTCGCAAATCTAAATCGGCT	Reverse primer for RNA editing analysis for site *rpoC1-497*
cox2-F	ATMG00160	GTTCTAAAATGGTTATTCCTCACA	Forward primer for RNA editing analysis for sites *cox2-138,278,379*
cox2-R	ATMG00160	GTTTGGGGGATTAATTGATTGG	Reverse primer for RNA editing analysis for sites *cox2-138,278,379*
orfX-F	ATMG00570	CACTTTTAGCTTTGAATTACTTAT	Forward primer for RNA editing analysis for sites *orfX-145,173,161,164,361,364,406,407,409,412,505*
orfX-R	ATMG00570	ATTGATAGTTACTTTGCCAGGTTC	Reverse primer for RNA editing analysis for sites *orfX-145,173,161,164,361,364,406,407,409,412,505*
ClpD-alcA-F	AT5G51070	GCAGGTCGACGGATCCATGGAGGTGTTATCTACTTCC	Forward primer for amplifying the coding sequence of *ClpD* and *ClpD-GFP* for fusion with alcA promoter, including a BamHI site
ClpD-alcA-R	AT5G51070	TCAGCGTACCGAATTCCTATGCGATCGATGTTTTGTCTGT	Reverse primer for amplifying the coding sequence of *ClpD* for fusion with alcA promoter, including an EcoRI site
GFP-alcA-R		TCAGCGTACCGAATTCTTACTTGTACAGCTCGTCCAT	Reverse primer for amplifying the coding sequence of *ClpD-GFP* for fusion with alcA promoter, including an EcoRI site

ClpD-Fusion-S	AT5G51070	CTCAAGCTTCGAATTCTGATGGAGGTGTTATCTACTTCC	Forward primer for amplifying the coding sequence of *ClpD* for constitutive expression of *ClpD* or *ClpD-GFP* driven by CAMV 35S promoter, including an EcoRI site
oGZW309-clpD-A	AT5G51070	GGCAGCAGCCGGATCCCGCTATGCGATCGATGTTTTGTCTGT	Reverse primer for amplifying the coding sequence of *ClpD* (with stop codon) for constitutive expression of ClpD driven by CAMV 35S promoter, including a BamHI site
oGZW424-ClpD-F	AT5G51070	CTCAAGCTTCGAATTCTGATGGCTATAATCTTCTCTCAGAAGG	Forward primer for amplifying the coding sequence of ClpD without cTP for constitutive expression of *ΔTP-ClpD-GFP* driven by CAMV 35S promoter, including an EcoRI site
ClpD-Fusion-A	AT5G51070	GGCAGCAGCCGGATCCCG TGCGATCGATGTTTTGTCTGT	Reverse primer for amplifying the coding sequence of ClpD (without stop codon) for constitutive expression of *ClpD-GFP* and *ΔTP-ClpD-GFP* driven by CAMV 35S promoter, including a BamHI site
pC231-HOT1-F	AT1G74310	GAGACAGGATCCGAATTCATGAATCCAGAGAAATTCACAC	Forward primer for amplifying the coding sequence of HOT1 for constitutive expression driven by CAMV 35S promoter in ClpD-GFP line #5 background.
pC231-HOT1-R	AT1G74310	CCTCCACCTCCACTAGTATCCTCGATCATTTCCTCATTAT	Reverse primer for amplifying the coding sequence of HOT1 for constitutive expression driven by CAMV 35S promoter in ClpD-GFP line #5 background.

References:

1. Wu, G.Z. *et al.* Control of retrograde signalling by protein import and cytosolic folding stress. *Nat Plants* **5**, 525-538 (2019).
2. Szklarczyk, D. *et al.* STRING v10: protein-protein interaction networks, integrated over the tree of life. *Nucleic Acids Res* **43**, D447-452 (2015).
3. Shannon, P. *et al.* Cytoscape: a software environment for integrated models of biomolecular interaction networks. *Genome Res* **13**, 2498-2504 (2003).
4. Li, L. *et al.* Protein degradation rate in Arabidopsis thaliana leaf growth and development. *Plant Cell* **29**, 207-228 (2017).
5. Li, M. *et al.* Plant editosome database: a curated database of RNA editosome in plants. *Nucleic Acids Res* **47**, D170-D174 (2019).
6. Lurin, C. *et al.* Genome-wide analysis of Arabidopsis pentatricopeptide repeat proteins reveals their essential role in organelle biogenesis. *Plant Cell* **16**, 2089-2103 (2004).
7. Wu, G.Z. *et al.* Control of retrograde signaling by rapid turnover of GENOMES UNCOUPLED1. *Plant Physiol* **176**, 2472-2495 (2018).